



A new satellite-based indicator to identify spatiotemporal foraging areas for herbivorous waterfowl

Wei, J., Xin, Q., Ji, L., Gong, P., & Si, Y.

This is a "Post-Print" accepted manuscript, which has been published in "Ecological Indicators"

This version is distributed under a non-commercial no derivatives Creative Commons



([CC-BY-NC-ND](https://creativecommons.org/licenses/by-nc-nd/4.0/)) user license, which permits use, distribution, and reproduction in any medium, provided the original work is properly cited and not used for commercial purposes. Further, the restriction applies that if you remix, transform, or build upon the material, you may not distribute the modified material.

Please cite this publication as follows:

Wei, J., Xin, Q., Ji, L., Gong, P., & Si, Y. (2019). A new satellite-based indicator to identify spatiotemporal foraging areas for herbivorous waterfowl. *Ecological Indicators*, 99, 83-90. DOI: 10.1016/j.ecolind.2018.12.016

You can download the published version at:

<https://doi.org/10.1016/j.ecolind.2018.12.016>

1 **Title**

2 A new satellite-based indicator to identify spatiotemporal foraging areas for herbivorous
3 waterfowl

4

5 **List of Authors**

6 Jie Wei¹, Qinchuan Xin², Luyan Ji¹, Peng Gong¹, Yali Si^{1,3,*}

7

8 **Author Affiliations**

9 ¹ Ministry of Education Key Laboratory for Earth System Modeling, and Department of
10 Earth System Science, Tsinghua University, Beijing 100084, China

11 ² Guangdong Provincial Key Laboratory of Urbanization and Geo-simulation, Sun Yat-sen
12 University, Guangzhou 510275, China

13 ³ Resource Ecology Group, Wageningen University, Droevendaalsesteeg 3a, 6708 PB
14 Wageningen, The Netherlands

15

16 **Author Emails**

17 Jie Wei (weij16@mails.tsinghua.edu.cn)

18 Qinchuan Xin (xinqinchuan@gmail.com)

19 Luyan Ji (jily@mail.ustc.edu.cn)

20 Peng Gong (penggong@mail.tsinghua.edu.cn)

21 Yali Si (yalisi@mail.tsinghua.edu.cn); Corresponding author

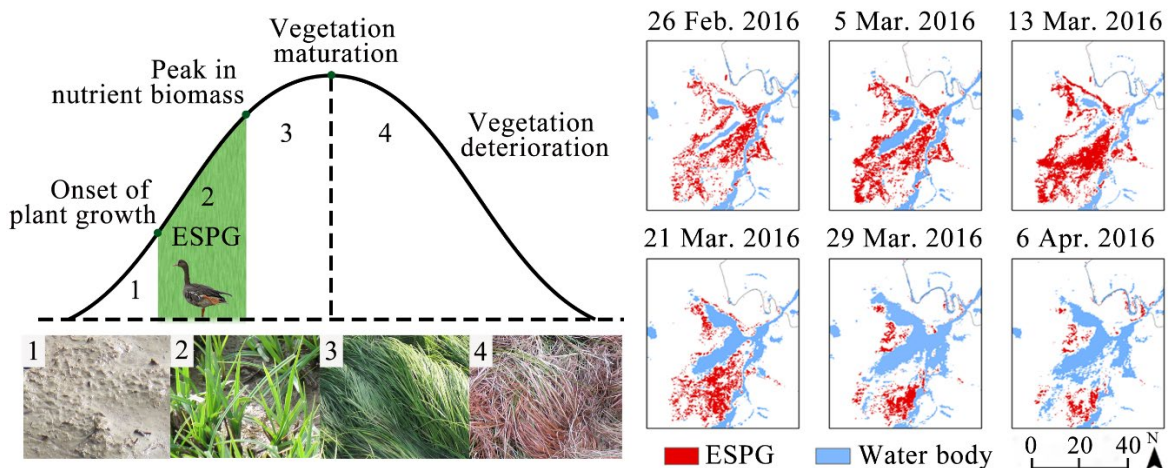
22 **Abstract**

23 The distribution of food resources is a key factor in habitat selection. Herbivorous waterfowl
24 prefer early-stage growing plants (from the onset of plant growth to the peak in nutrient
25 biomass) as these offer higher energy intake rates. This plant development stage is not fully
26 captured by commonly used satellite-derived vegetation indicators, which focus on plant
27 biomass (e.g., Enhanced Vegetation Index, EVI) or active plant growth (e.g., the differential
28 EVI between current and a previous date, diffEVI). To improve mapping suitable grazing
29 areas for herbivorous waterfowl, we propose a new satellite-based plant growth indicator of
30 early-stage plant growth (ESPG). We assume herbivorous waterfowl prefer plants at an early
31 development stage during the growing season and select plants with a relatively later end of
32 ESPG during the non-growing season. We use satellite tracking data of 20 greater white-
33 fronted geese (*Anser albifrons*) wintering in the Yangtze River floodplain to validate our
34 predictions. We build generalized linear models for goose distributions during the growing
35 and non-growing seasons and compare the performance of ESPG to commonly used plant
36 growth indicators (EVI and diffEVI). During the growing season, ESPG can explain 53% of
37 variation in the goose distribution, outperforming EVI (27%) and diffEVI (34%). During the
38 non-growing season, only the end of ESPG significantly influences goose distribution,
39 explaining 25% of the variability (ESPG: AUC = 0.78; EVI: AUC = 0.58; diffEVI: AUC =
40 0.58). The newly-developed plant growth indicator ESPG could be used to improve models
41 of herbivorous waterfowl distributions and hence support efforts toward waterfowl
42 conservation and wetland management.

43 **Keywords**

44 Geese; Distribution; Yangtze River floodplain; MODIS; Nutrient biomass; Plant phenology

45 **Graphical abstract**



46

47 **Highlights**

- 48 1. Herbivorous waterfowl select early-stage growing plants to maximize energy intake.
- 49 2. A newly-proposed ESPG metric outperforms other plant growth indicators.
- 50 3. ESPG could improve bird distribution modelling and support wetland management.

51 1. Introduction

52 Food provides the principal energy for activities crucial to individual survival and
53 population recruitment (Newton, 1980). Food availability is regarded as a key factor in
54 species habitat choice (Dussault et al., 2005; Hutto, 1985; Johnson and Sherry, 2001).
55 Herbivorous waterfowl tend to alter their distribution according to spatial and temporal
56 variations of food availability at both site (Pedrana et al., 2011; Wu et al., 2014) and flyway
57 levels (Si et al., 2015a; Si et al., 2015b; van der Graaf et al., 2006). Therefore, accurate
58 measurements of food availability are critical for wetland management and waterfowl
59 conservation.

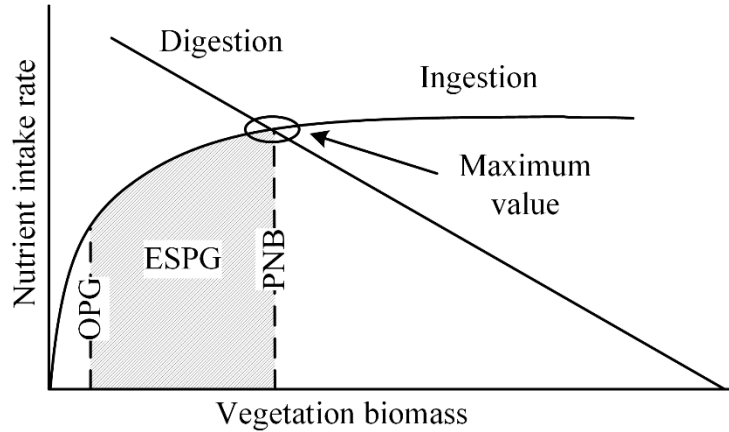
60 Herbivorous waterfowl are selective feeders due to their limited digestion capability,
61 preferring young and nutritious plants (Bos et al., 2005; Mattocks, 1971; Prop and Vulink,
62 1992). Food intake rates increase as plants develop and add biomass; however, digestibility
63 decreases because the fractional content of less-digestible fibrous material increases as plant
64 tissues mature (Hassall, 2001; Mowat et al., 1965; Riddington et al., 1997). Hence birds must
65 balance forage quantity against quality to maximize their nutrient intake.

66 Satellite-based vegetation indicators have been developed to measure the ‘greenness’ of
67 the vegetation canopy (Garrouette et al., 2016; Kerr and Ostrovsky, 2003; Pettorelli et al.,
68 2005). The Normalized Difference Vegetation Index (NDVI) is most frequently used, for
69 example for investigating shifts in the duration of the growing season (Piao et al., 2006), and
70 calculating the rate of greenup and senescence of vegetation (Reed and Ohlen, 1994).
71 However, NDVI is sensitive to soil background brightness, as well as atmospheric
72 contaminants, and is saturated at areas with a high vegetation biomass (Jiang et al., 2008).
73 To overcome these problems, the Enhanced Vegetation Index (EVI) has been proposed to
74 improve the monitoring of vegetation productivity (Jiang et al., 2008). NDVI and EVI has
75 been frequently used as the surrogate of food to predict the distribution and movement of
76 avian herbivores (Gottschalk et al., 2005; Si et al., 2015b). Positive effects have been found
77 between these indicators and bird abundance or richness (Guan et al., 2016; Wu et al., 2014).
78 Furthermore, Bridge et al. (2015) proposed an indicator based on the differential EVI
79 (diffEVI), defined as the change in EVI on monthly time scales, to measure increases in
80 vegetation biomass. Their results showed that painted buntings (*Passerina ciris*) maximize
81 consumption of new plant growth during their autumn migration.

82 Traditional satellite-derived indicators are widely used in bird ecology, because their
83 calculation is straightforward and many standard products are freely available. For example,
84 NDVI is defined as the ratio of the difference between near-infrared reflectance and red
85 visible reflectance to their sum. Vegetation index products like 250-m Moderate Resolution
86 Imaging Spectroradiometer (MODIS) NDVI and EVI and 1-km Advanced Very High
87 Resolution Radiometer (AVHRR) NDVI are free to download. However, NDVI and EVI
88 only quantify the biomass but not the vegetation quality, and a greater value of NDVI or EVI
89 represent a higher amount of biomass and more advanced plant development (Guan et al.,
90 2016; Pedrana et al., 2011; Somveille et al., 2018). Though diffEVI considers the amount of
91 newly grown plants (Bridge et al., 2015; Li et al., 2017; Zhang et al., 2018), it cannot take
92 the plant quality properly into account, as plant digestibility decreases when biomass
93 increases. Therefore, none of these metrics can accurately quantify the potential foraging
94 areas for herbivorous waterfowl.

95 The forage maturation hypothesis suggests that the highest nutrient intake rate is defined
96 by the intersection of food ingestion and digestibility constraints, corresponding to plant
97 development stages with low to intermediate biomass (Drescher et al., 2006; Fryxell, 1991;
98 Si et al., 2011). Furthermore, taller and more mature plants are more difficult for birds to
99 crop, chew and swallow (Durant et al., 2003; Heuermann et al., 2011). Therefore, herbivorous

100 waterfowl prefer early-stage plant growth (ESPG) with low or intermediate biomass, since
 101 such plants offer the highest nutrient intake rates (Fig. 1). We define the start of ESGP as the
 102 onset of the plant growth and the end of ESGP as the time when plants reach peak nutrient
 103 biomass, with the latter quantified as the highest amount of nitrogen per unit area (Si et al.,
 104 2015a; van der Graaf et al., 2006).
 105



106
 107 Fig. 1. The maximum nutrient intake rate under forage ingestion and digestion constraints
 108 and its relationship with the early-stage plant growth (ESPG) period. ESGP is defined as
 109 extending from the onset of plant growth (OPG) to the peak in nutrient biomass (PNB, the
 110 highest amount of nitrogen per unit area).
 111

112 In order to capture the dynamic change of vegetation development, it is necessary to
 113 acquire satellite images with relatively high spatial and temporal resolutions, especially for a
 114 high temporal resolution. The high spatial-resolution imagery, such as 30-m Landsat and 10-
 115 m Sentinel-2, are frequently contaminated by clouds, resulting in a relatively low temporal
 116 resolution of available images. The biweekly 250-m MOIDS and 1-km AVHRR vegetation
 117 index products also have a relatively low temporal resolution. Considering the trade-off
 118 between the temporal and spatial resolution, we adopt the 250-m 8-day EVI calculated using
 119 MODIS surface reflectance products.

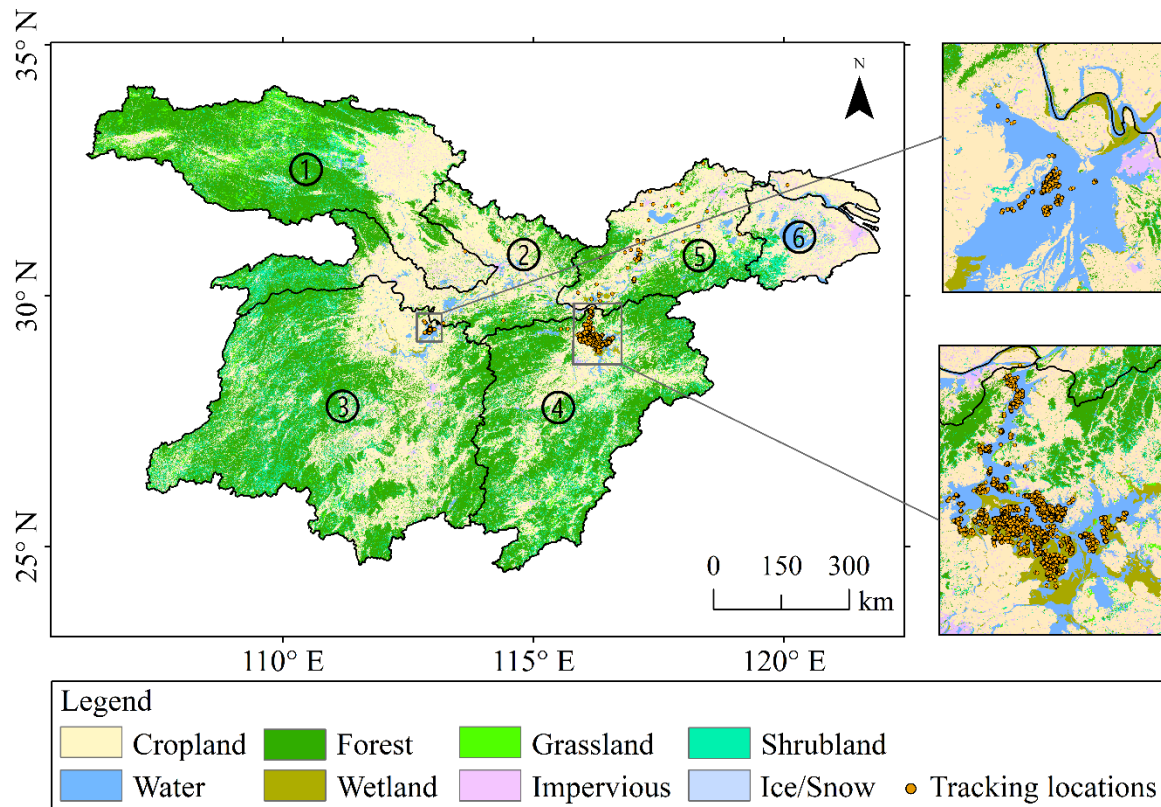
120 In this study, we propose a new satellite-based indicator of ESGP to map the
 121 spatiotemporal variation in suitable foraging area for herbivorous waterfowl. We hypothesize
 122 that waterfowl prefer plants at an earlier development stages during the growing season and
 123 select plants with the latest ESGP during the non-growing season. Using satellite tracking
 124 data of greater white-fronted geese (*Anser albifrons*) on the Yangtze River floodplain, we
 125 build generalized linear models to predict goose distributions using ESGP, EVI, and diffEVI,
 126 respectively. We then compare the performances of these indicators during both the growing
 127 and non-growing seasons.

128 2. Materials and Methods

129 2.1. Study area

130 The middle and lower Yangtze River floodplain are composed of six drainage basins,
 131 the Hanjiang River, the Yichang-Hukou middle mainstream section, Dongting Lake, Poyang
 132 Lake, the lower mainstream section, and Tai Lake (Fig. 2), with an area of about 8×10^5 km².
 133 The plain experiences a subtropical monsoon climate, with an annual mean precipitation of
 134 1000-1400 mm and an annual mean temperature of 14-18 °C (Xie et al., 2017). In addition
 135 to the two main freshwater lakes of Poyang and Dongting Lake, numerous smaller freshwater

136 lakes, ponds, and reservoirs are distributed across the plain. In total, these water bodies
 137 comprise about 25% of the freshwater lake area in East Asia (Wang et al., 2014). The
 138 hydrological characteristic of summer flooding and winter drought produces extensive
 139 seasonal wetland meadows. The dominant plant families are Cyperaceae (e.g., *Carex spp.*)
 140 and Gramineae (e.g., *Triarrhena lutarioriparia* and *Phalaris arundinacea*). Grass-eating
 141 waterfowl mainly forage on *Carex spp.*, such as *Carex heterolepis* (Zhao et al., 2012).



142
 143 Fig. 2. Satellite tracking locations for greater white-fronted geese (*Anser albifrons*) from
 144 autumn 2015 to spring 2016 in the middle and lower Yangtze River floodplain. The land
 145 cover map is based on 30-m Finer Resolution Observation and Monitoring of Global Land
 146 Cover (FROM-GLC) data for 2010. The six drainage basins are ① Hanjiang River, ②
 147 Yichang-Hukou middle mainstream section, ③ Dongting Lake, ④ Poyang Lake, ⑤ the
 148 lower mainstream section, and ⑥ Tai Lake.

149 2.2. Data

150 2.2.1. Remote sensing data

151 MODIS Terra surface reflectance products (MOD09Q1) for the period of 2015-2016
 152 were acquired from an open online gateway (<https://e4ftl01.cr.usgs.gov>) to calculate EVI.
 153 The dataset consists of 8-day level-3 products at a spatial resolution of 250 m. To extract the
 154 start and end of the thermal growing seasons of the seasonal wetland meadows, we also adopt
 155 MODIS Aqua level-3 land surface temperature (LST) products (MYD11A2) for 2015-2016
 156 from the same gateway, which are provided at a 1-km spatial resolution and an 8-day
 157 temporal resolution. LST affects vegetation growth more directly than the air temperature as
 158 it is derived from the thermal-infrared radiance, and measures the canopy temperature at
 159 vegetated areas and the soil temperature at barren areas (Wan and Dozier, 1996). Land use
 160 information for bird locations and downstream analyses is based on 30-m Finer Resolution
 161 Observation and Monitoring of Global Land Cover (FROM-GLC) data for 2010, acquired

162 from http://data.ess.tsinghua.edu.cn/data/temp/China_LC_update_v5/ (Gong et al., 2013; Yu
163 et al., 2017).

164 2.2.2. *Bird tracking data*

165 During 30 January-2 February and 7-16 December 2015, twenty greater white-fronted
166 geese are captured and fixed with a solar-powered GPS-GSM (Global Positioning System-
167 Global System for Mobile Communications) neck transmitter at Poyang Lake, Jiangxi
168 province, China (29.15°N, 116.10°E). A total of 10 IBIS series loggers (22g, Ecotone
169 Telemetry, Gdynia, Poland) and 10 HQNG series loggers (26g, Hunan Global Messenger
170 Technology Co. Ltd., Xiangtan, China) are used. The weight of these transmitters represents
171 less than 1% of the average body weight among the tracked geese (2122 ± 226 g, mean \pm
172 standard deviation). The transmitters are set to record GPS positions every two hours.
173 Detailed capture and deploy methods have been provided by Si et al. (2018). From the
174 autumn of 2015 to the spring of 2016, a total of 13,819 locations are collected over the
175 Yangtze flood plain (Table S1). All tracking data are archived in Movebank
176 (www.movebank.org) under ID 52997422, study ‘2015 Tsinghua waterfowl (Yangtze)’.

177 2.3. *Methods*

178 2.3.1. *Preprocessing satellite imagery*

179 We calculate a two-band Enhanced Vegetation Index to characterize plant growth (Jiang
180 et al., 2008) by equation:

$$EVI = 2.5 \frac{N - R}{N + 2.4R + 1} \quad (1)$$

181 where N and R represent surface reflectance in the near-infrared and red bands, respectively.
182 To reduce noise, a Savitzky-Golay fitting method with a window size of 4 is used to smooth
183 the EVI time series via TIMESAT software (Eklundh and Jönsson, 2015; Jönsson and
184 Eklundh, 2002, 2004). Based on quality control information provided with the satellite
185 imagery, observations with cloud contamination are assigned a weight of zero and
186 observations without cloud contaminations a weight of one.

187 Permanent water and permanent non-vegetated areas are removed from the maximum
188 flood area to better isolate potential foraging area. We first generate a dynamic 8-day water
189 mask for 2015–2016 from surface reflectance data using an automated procedure that can
190 deal with mountain and cloud shadows, as well as spectral mixing at the water-land boundary
191 (Ji et al., 2015). The maximum flood area is then derived by stacking these 8-day water masks
192 together. Pixels classified as water for the whole year (46 images) are defined as permanent
193 water. Pixels with the smoothed EVI values less than 0.2 (Bhandari et al., 2012) for the whole
194 growing season are defined as permanent non-vegetated areas. The potential foraging area is
195 then obtained by removing the permanent water and non-vegetated areas from the maximum
196 flood area. Using EVI to remove non-vegetated areas is independent of the following
197 analyses, thereby would not influence the comparison of three indicators (ESPG, EVI, and
198 diffEVI) as we only evaluate their ability in predicting bird distribution in the potential
199 foraging areas.

200 The start and end of the growing season for seasonal wetland meadows on a floodplain
201 are determined by water levels and local temperature. To explore changes in water levels
202 during 2015-2016, water area is defined as the sum of water pixels in each 8-day water mask.
203 As the spring growing season for wetland meadows ends when flooded, we consider the date
204 with the largest water area to be the end of the spring growing season. A seven-order
205 polynomial fit is then performed between the water area and the corresponding Julian day to
206 obtain a fit to the annual cycle (the water time-series curve). As the autumn growing season

207 starts when floods recess, the maximum negative rate of change in this curve (the date of
208 fastest flood recession) is considered as the start of the autumn growing season.

209 It has been suggested that vegetation can only germinate when daily average
210 temperatures are at least 5°C for five consecutive days (Frich et al., 2002). We therefore
211 interpolate the 8-day land surface temperature data to obtain a daily time series for each pixel,
212 and identify when the daily temperature dipped below 5°C for five consecutive days in
213 autumn 2015 (the end of the autumn growing season per pixel), as well as when the daily
214 temperature exceeded 5°C for five consecutive days in spring 2016 (the start of the spring
215 growing season per pixel). The end of the autumn growing season for the Yangtze River
216 floodplain is defined as the median of the end dates for all pixels in the study area. The start
217 of the spring growing season in 2016 is similarly defined as the median of the start dates for
218 all pixels in the study area. According to these definitions, the autumn 2015 growing season
219 extended from 13 August to 25 November, and the spring 2016 growing season from 26
220 February to 13 June.

221 2.3.2. *Deriving the spatiotemporal distribution of early-stage plant growth (ESPG)*

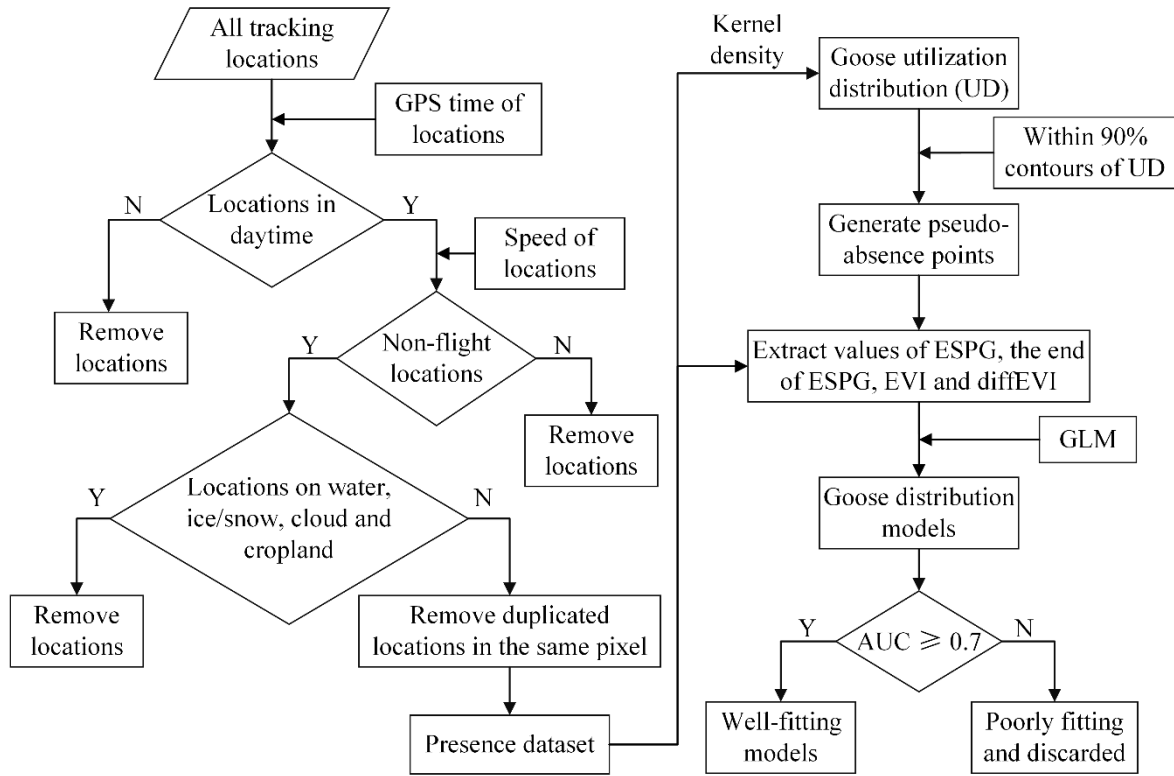
222 To identify the onset dates for plant growth and the peaks in nutrient biomass for the
223 autumn and spring growing seasons, we calculate the change rate (*CR*) in the EVI time series
224 by equation (2):

$$CR = \frac{EVI_{n+1} - EVI_n}{d} \quad (2)$$

225 where *n* ranges from 1 to the last EVI imagery of the growing season and *d* is the time interval
226 between two consecutive images. Given the 8-day temporal resolution of the EVI imagery,
227 the value of *d* is set to eight. The onset of plant growth is defined as the date with the highest
228 positive rate (Reed and Ohlen, 1994; Si et al., 2015a). After the onset of plant growth, the
229 date that vegetation growth ceased is defined as the first time the change rate is equal or less
230 than zero. The peak in nutrient biomass is then calculated as the middle date between the
231 onset of plant growth and the date that growth ceased (Si et al., 2015a). Dates between the
232 onset of plant growth and the peak in nutrient biomass are considered as ESPG, and the value
233 of the ESPG indicator is set to 1 (suitable foraging area). Otherwise the value of the ESPG
234 indicator is set to 0 (unsuitable). We then generate 8-day ESPG indicator maps for both
235 growing seasons to support downstream analyses.

236 2.3.3. *Preprocessing bird tracking data*

237 A series of data preprocessing steps are executed for the bird tracking data (Fig. 3).
238 Greater white-fronted geese are mainly diurnal feeders (though some night feeding has been
239 reported under bright moonlight (Ely, 1992)). Therefore, we first consider only non-flight
240 tacking locations during daytime, where daytime is defined as the period from one hour
241 before sunrise to one hour after sunset. Sunrise and sunset times are calculated based on the
242 geographic coordinates of each tracking location using algorithms provided by the National
243 Oceanic & Atmospheric Administration (NOAA)
244 (<https://www.esrl.noaa.gov/gmd/grad/solcalc/>). The selection of specific plant conditions
245 does not apply to cropland or water pixels, so we exclude tracking points corresponding to
246 these land cover types from further analysis (only 1% of tracking locations were cropland).
247 Locations on snow/ice and under cloud cover are also removed from the analysis.
248 Furthermore, to avoid pseudo-replication, only one bird record is kept when multiple records
249 correspond to the same pixel (Zhang et al., 2018).



250

251 Fig. 3. The flow chart of preprocessing bird tracking data and comparing the performance of
 252 early-stage plant growth (ESPG) with enhanced vegetation index (EVI) and the differential
 253 EVI (diffEVI). GLM: generalized linear model; AUC: Area Under the Curve of the Receiver
 254 Operation Characteristic metric.

255 *2.3.4. Comparing the performance of ESPG with EVI and diffEVI*

256 For the growing and non-growing season, we adopt ESPG and the end of ESPG as a
 257 proxy for food availability. We also calculate other proxies, including EVI and diffEVI, and
 258 evaluate the ability of each proxy to predict the goose distribution. EVI is generated from the
 259 8-day surface reflectance product. DiffEVI is calculated by subtracting the value of EVI one
 260 month prior from the current value (Bridge et al., 2015).

261 We build a generalized linear model (GLM) with a log-link function using ESPG, the
 262 end of ESPG, EVI, and diffEVI respectively, to predict goose distributions during the
 263 growing and non-growing seasons (Fig. 3). We first generate pseudo-absence data to
 264 facilitate building the model. We apply the kernel density method to estimate the goose
 265 utilization distribution (UD) using the package ‘adehabitatHR’ in R 3.3.3. Then, pseudo-
 266 absences with a number of equal to the number of presences are randomly generated within
 267 the 90% contours of the UD (Li et al., 2017) under the constraint that no pseudo-absence
 268 point is created in areas corresponding to water, clouds or ice or within 1 km of a presence
 269 point. Since all presence data are associated with a specific date, dates are allocated randomly
 270 within the growing or non-growing season for each pseudo-absence point. Accounting for
 271 plant conditions in surrounding pixels, we generate a 250-m buffer around each presence or
 272 pseudo-absence point and extract vegetation conditions from the 8-day vegetation maps
 273 corresponding most closely to the timing of that point. If at least one pixel of the ESPG map
 274 within the buffer equals one, we regard that location as under early-stage plant development.
 275 For the end of ESPG, EVI and diffEVI, we use the median values within the buffer. We
 276 repeat this procedure 1000 times to minimize any influences of randomly generating pseudo-
 277 absence points, thus creating 1000 GLM models for each indicator during the growing season,
 278 and 1000 models for the non-growing season. When constructing each GLM model, 80% of

279 the points are chosen randomly to train the model and the remaining 20% of the points are
280 used for model validation.

281 We evaluate model performance using the Area Under the Curve (AUC) of the Receiver
282 Operation Characteristic (ROC) metric. Models with an AUC value less than 0.7 are regarded
283 as poorly fitted (Li et al., 2017; Swets, 1988) and discarded from the analysis. We then use
284 the well-fitting models for each indicator to estimate the mean and standard deviation of each
285 model parameter. We assess the relative utility of each plant growth indicator using the R-
286 squared metric as an estimate of the amount of variance in the response variable explained
287 by the given predictor. Response functions for plant growth indicators with significant effects
288 ($p < 0.05$) are constructed by using the prediction model to estimate the response value (and
289 the 95% confidence interval) across the range of interest.

290 **3. Results**

291 *3.1. Spatiotemporal distribution of early-stage plant growth*

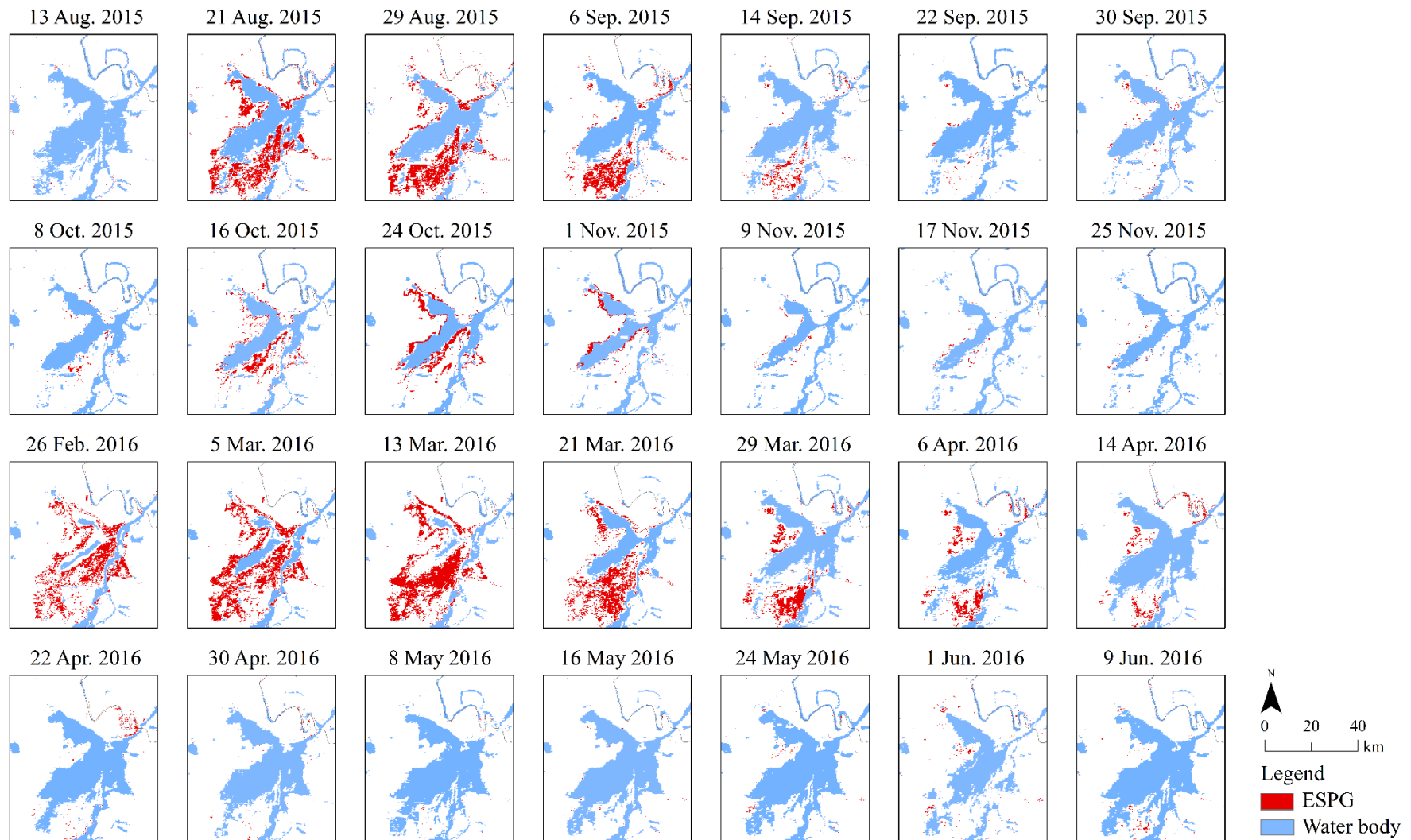
292 Spatiotemporal 8-day ESPG maps for herbivorous waterfowl in the middle and lower
293 Yangtze River floodplain were generated during the growing season from 2015 August to
294 2016 June (Fig. S1). ESPG showed similar spatial and temporal variations at the key sites,
295 Dongting Lake (Fig. 4) and Poyang Lake (Fig. 5). Following the flood recession, ESPG
296 increased steeply from late August to mid-September during the 2015 autumn growing
297 season. The area of ESPG reached its maximum extent on 21 August for about 406 km² at
298 Dongting Lake, and on 6 September for about 1438 km² at Poyang Lake. During the 2016
299 spring season, ESPG availability was greatest during the period from late February to late
300 March. The maximal ESPG area was found on 13 March at both Dongting Lake (545 km²)
301 and Poyang Lake (450 km²). The area of ESPG decreased rapidly with the increase of
302 flooding area from the middle April.

303 *3.2. Performance of different plant growth indicators*

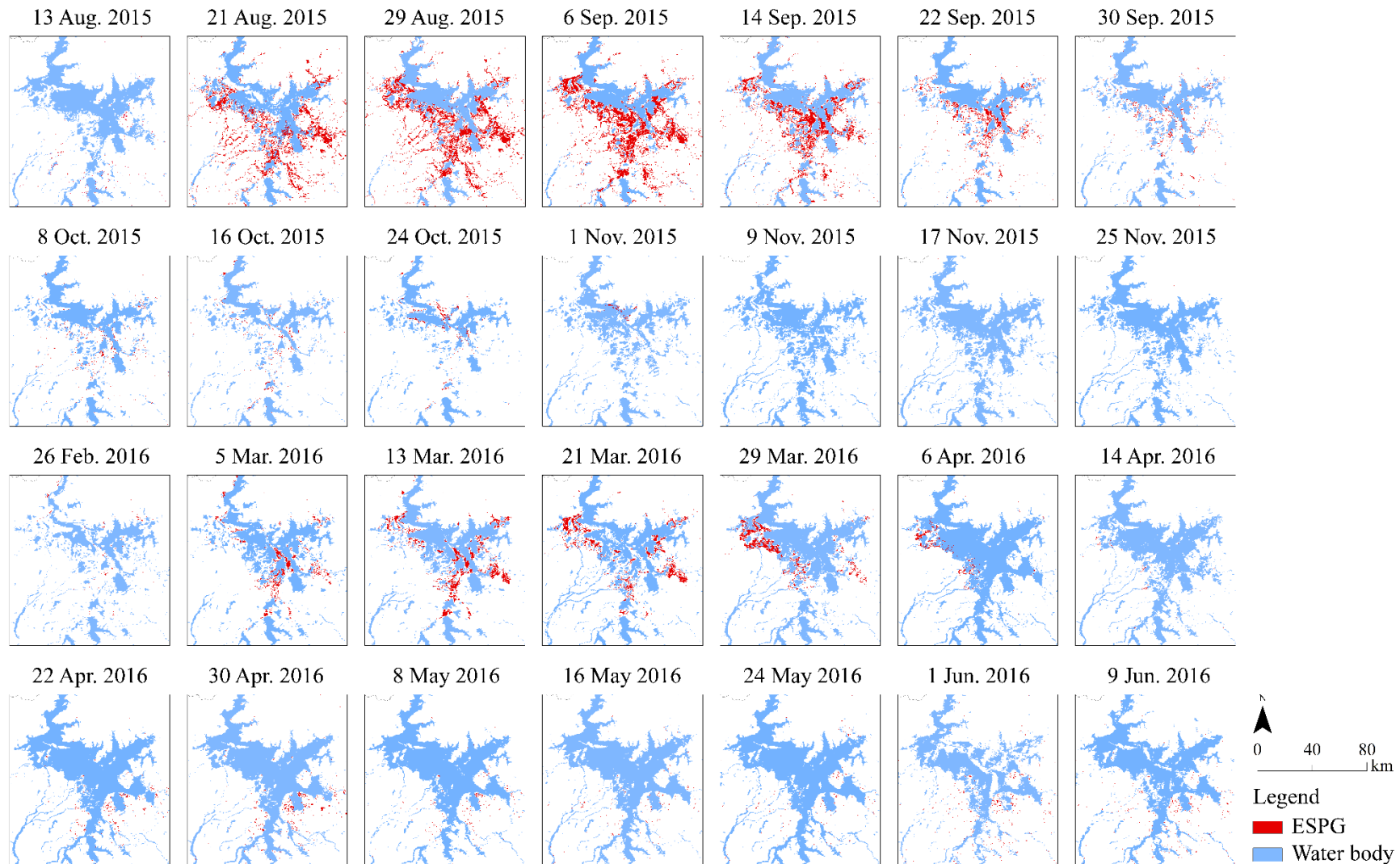
304 During the growing season, ESPG, EVI and diffEVI could all successfully predict the
305 spatial distribution of greater white-fronted geese in the middle and lower Yangtze River
306 floodplain (AUC > 0.7, $p < 0.05$, Table 1). The probability of bird occurrence was highest
307 when ESPG was available (Fig. 6a), while EVI was negatively related and diffEVI was
308 positively related with goose occurrence (Fig. 6b-c). ESPG can explain 55% of the variance
309 in the goose distribution during the growing season, which is more than by the other
310 indicators (27% for EVI and 34% for diffEVI; Table 1).

311 During the non-growing season, only the end of ESPG had a significant relationship
312 with goose distribution (AUC = 0.78, $p < 0.05$; Table 1). The model suggested that geese
313 preferred to forage during the wintering and spring-staging periods in areas with a later end
314 of ESPG (Fig. 6d). EVI and diffEVI could not accurately predict the goose distribution during
315 this period (AUC < 0.7, Table 1).

316



317
 318 Fig. 4. Spatiotemporal distributions of early-stage plant growth (ESPG) and water bodies at Dongting Lake in the middle and lower Yangtze River
 319 floodplain during the 2015 autumn and 2016 spring growing seasons.



320
321
322

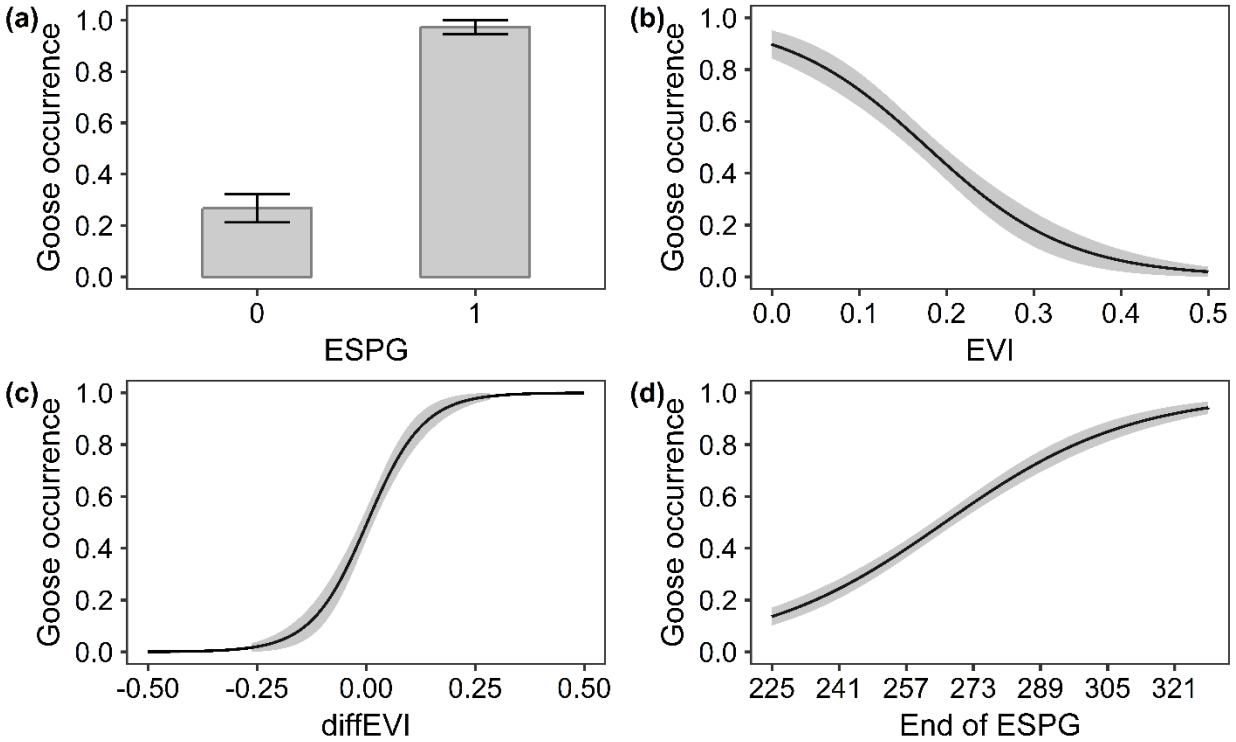
Fig. 5. Spatiotemporal distributions of early-stage plant growth (ESPG) and water bodies at Poyang Lake in the middle and lower Yangtze River floodplain during the 2015 autumn and 2016 spring growing seasons.

323 Table 1. The performance of the early-stage plant growth (ESPG), enhanced vegetation index
 324 (EVI), and the differential EVI (diffEVI) metrics in predicting the distribution of greater white-
 325 fronted geese (*Anser albifrons*) in the middle and lower Yangtze River floodplain (mean \pm standard
 326 deviation of 1000 models with randomly-assigned absence points; see text for further details).

Period	Variable	AUC	p	R^2
Growing season	ESPG	0.83 \pm 0.01	< 0.001 \pm < 0.001	0.55 \pm 0.03
	EVI	0.72 \pm 0.02	< 0.001 \pm < 0.001	0.27 \pm 0.03
	diffEVI	0.79 \pm 0.04	< 0.001 \pm < 0.001	0.34 \pm 0.04
Non-growing season	End of ESGP	0.78 \pm 0.02	< 0.001 \pm < 0.001	0.25 \pm 0.02
	EVI	0.58 \pm 0.03*	-	-
	diffEVI	0.58 \pm 0.02*	-	-

327 * Indicating that AUC values for all 1000 models were less than 0.7.

328



329

330

331

332

333

Fig. 6. Relationships between goose occurrence and plant growth indicators during the growing
 season (a-c) and non-growing season (d). Grey areas indicate 95% confidence intervals. ESGP:
 early-stage plant growth; EVI: enhanced vegetation index; diffEVI: difference between EVI at
 the current time and EVI one month prior.

334 **4. Discussion**

335

336

337

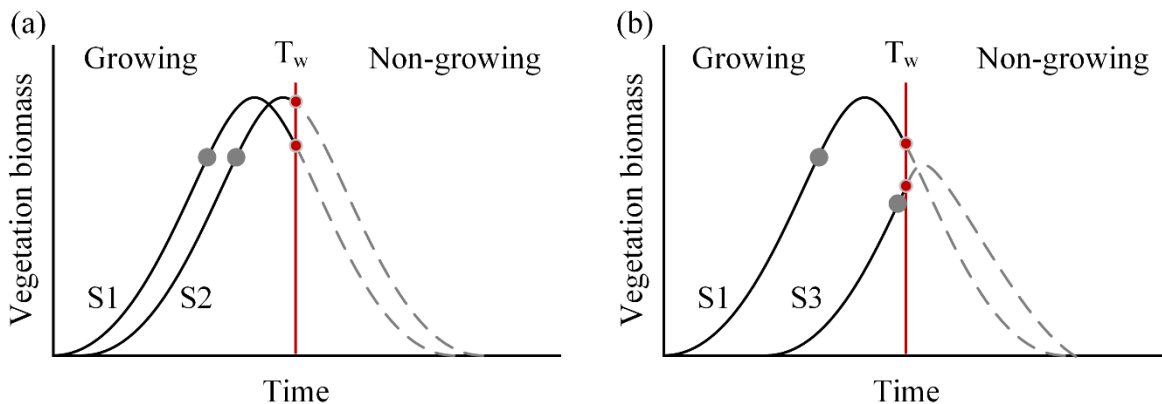
338

We propose a new indicator of early-stage plant growth (ESPG) to identify suitable foraging
 areas for herbivorous waterfowl. We determine the spatiotemporal distribution of ESGP in the
 middle and lower Yangtze River floodplain. We then compare the performance of ESGP with the
 traditional plant growth indicators (EVI and diffEVI) for predicting the waterfowl distribution

339 using satellite-based goose tracking data and generalized linear models. We find that the model
340 based on ESGP best predicts the bird distribution during the growing season, while the end of
341 ESGP is the only indicator that significantly influences bird distribution during the non-growing
342 season.

343 Satellite-derived ESGP is a powerful proxy indicator of suitable forage areas for herbivorous
344 waterfowl. ESGP represents plants in the stage between the onset of plant growth and the peak in
345 nutrient biomass, and therefore accounts for both the quantity and quality of forage. Nutrient intake
346 rates for herbivorous waterfowl increase substantially during this stage. Continued increase in the
347 fiber content of leaves and stems means that plants become less palatable and less digestible after
348 this period, resulting in sharp decreases in nutrient intake rates (Drescher et al., 2006; van der Wal
349 et al., 1998). Geese might consistently graze on one forage area to prolong the early-stage plant
350 growth period (Bos et al., 2004; Fryxell, 1991; van der Graaf et al., 2005). Furthermore, areas
351 grazed by livestock would be more preferred by geese, since grazing could create fresh new plant
352 with a lower height and a higher quality (van der Graaf et al., 2002). EVI and diffEVI are also
353 linked to goose distribution, in accordance with previous findings (Li et al., 2017). However, when
354 other environmental variables (e.g., climate, topography and human disturbance) are incorporated
355 in models for predicting bird distributions, EVI and diffEVI are relatively unimportant (Li et al.,
356 2017), in some cases even contributing less than 1% (Zhang et al., 2018). We suggest that including
357 ESGP in herbivorous waterfowl species distribution models could help to improve the predictive
358 power of such models.

359 During the non-growing season, geese favored areas with a later end of ESGP. As winter
360 approaches and temperatures drop, plants at almost all development stages cease growth and start
361 to deteriorate. Plants with a later peak in nutrient biomass means are relatively young and fresh,
362 and may therefore sustain a relatively higher quality during winter. However, a higher biomass
363 during the non-growing season does not necessarily correspond to a higher quality of forage. If all
364 plants have reached maturity before the start of the non-growing season, a higher biomass (i.e., a
365 lower deterioration level) might indicate a relatively higher quality (Fig. 7a). Yet, plants that have
366 not reached maturity but ceased growing solely because of the advent of low temperatures (i.e.,
367 plants with a later end of ESGP), might have a relatively higher quality despite a lower total
368 biomass (Fig. 7b). Traditional plant growth metrics (EVI and diffEVI) mainly depict biomass
369 variation or accumulation and hence are unsuitable indicators of potential foraging land during the
370 non-growing season. The date of ESGP should be included among core environmental data layers
371 when predicting distributions of herbivorous waterfowl, especially during the non-growing season.



372 Fig. 7. Schematic figures illustrating seasonal variation of plant biomass. Plants at three sites (S1,
373 S2 and S3) cease growth at different times. When entering the non-growing period, S2 has a
374

375 relatively higher biomass and quality in comparison to S1 (a), while S3 has a relatively lower
376 biomass but a higher quality in comparison to S1 (b). T_w indicates the start of the non-growing
377 season. Grey solid circles indicate the end of early-stage plant growth (ESPG).
378

379 Herbivorous waterfowl populations are vulnerable to wetland degradation and loss, and can
380 be regarded as a sensitive bioindicator of the health of wetland ecosystems (de Boer et al., 2011;
381 Kays et al., 2015). Our study supports the hypothesis that herbivorous waterfowl select early-stage
382 growing plants due to a trade-off between forage quantity and quality. The generated
383 spatiotemporal distributions of suitable forage area maps are critical for real-time monitoring and
384 instantaneous intervention. Targeted measures could be applied to the core foraging areas to
385 increase the habitat quality. For example, shortages of suitable food during the growing season
386 could be improved by mowing plants to prolong the ESGP period and create young and high-
387 quality food for herbivorous waterfowl. The proposed plant growth indicator ESGP identifies
388 plants at a stage suitable for consumption by herbivorous waterfowl and is therefore a superior
389 indicator for predicting waterfowl distributions relative to previously-proposed forage surrogates
390 derived from satellite data. Spatiotemporal distribution modelling of herbivorous waterfowl could
391 be improved using ESGP, and thereby provide important information for a better understanding of
392 the impact of a fast-changing environment on these species, and offer more effective protection
393 measures to safeguard waterfowl populations. In the future, when new satellite data with higher
394 spatial and temporal resolutions become available, EPSG could be even more accurately captured
395 and applied in herbivore conservation.

396 **5. Conclusions**

397 Herbivorous waterfowl balance food quantity and quality by foraging on plants in the early-
398 stage growth period to achieve higher rates of nutrient intake. Comparing the performance of a
399 newly-proposed indicator of early-stage plant growth (ESPG) to those of traditional plant growth
400 indicators (EVI and diffEVI), we find that ESGP (and the end of ESGP) outperform other
401 indicators in predicting goose distributions during both the growing and non-growing seasons.
402 ESGP could be used to monitor the spatiotemporal distribution of suitable foraging area for
403 herbivorous waterfowl, and could be integrated in species distribution models to improve the
404 accuracy of bird distribution predictions. The ESGP metric is easy to use and is a potentially
405 valuable tool for waterfowl conservation and wetland management applications.

406 **Acknowledgements**

407 This research was funded by the National Natural Science Foundation of China (Grant No.
408 41471347). We thank Guanhua Liu, Hao Luo, John Takekawa, Sivananintha Balachandran, Yanjie
409 Xu, Fei Xu, Wenyuan Zhang, Zhiyuan Lv and Wenzhao Wu for helping with bird tracking,
410 Yaomin Zheng for providing the boundary of the Yangtze River basins, and Ben Wielstra,
411 Jonathon S. Wright and Shenglai Yin for insightful comments and discussion.

412 **Supplementary Materials**

413 The following materials are available online. Fig. S1: Spatiotemporal distributions of early-
414 stage plant growth (ESPG) in the middle and lower Yangtze River floodplain during the 2015
415 autumn and 2016 spring growing seasons. Table S1: Summary of satellite tracking records for
416 each individual greater white-fronted goose (*Anser albifrons*) from 2015 autumn to 2016 spring in
417 the middle and lower Yangtze River floodplain.

418 **References**

- 419 Bhandari, A.K., Kumar, A., Singh, G.K., 2012. Feature Extraction using Normalized Difference
420 Vegetation Index (NDVI): a Case Study of Jabalpur City, in: Jena, S.K., Majhi, B. (Eds.), 2nd
421 International Conference on Communication, Computing & Security [Icccs-2012]. Elsevier
422 Science Bv, Amsterdam, pp. 612-621.
- 423 Bos, D., Drent, R.H., Rubinigg, M., Stahl, J., 2005. The relative importance of food biomass and
424 quality for patch and habitat choice in Brent Geese *Branta bernicla*. *Ardea* 93, 5-16.
- 425 Bos, D., van de Koppel, J., Weissing, F.J., 2004. Dark-bellied Brent geese aggregate to cope with
426 increased levels of primary production. *Oikos* 107, 485-496.
- 427 Bridge, E.S., Ross, J.D., Contina, A.J., Kelly, J.F., 2015. Do molt-migrant songbirds optimize
428 migration routes based on primary productivity? *Behavioral Ecology* 27, 784-792.
- 429 de Boer, W.F., Cao, L., Barter, M., Wang, X., Sun, M., Van, O.H., De, L.J., Barzen, J., Prins, H.H.,
430 2011. Comparing the community composition of European and eastern Chinese waterbirds and the
431 influence of human factors on the China waterbird community. *Ambio* 40, 68-77.
- 432 Drescher, M., Heitkonig, I.M.A., Van den Brink, P.J., Prins, H.H.T., 2006. Effects of sward
433 structure on herbivore foraging behaviour in a South African savanna: An investigation of the
434 forage maturation hypothesis. *Austral Ecol.* 31, 76-87.
- 435 Durant, D., Fritz, H., Blais, S., Duncan, P., 2003. The functional response in three species of
436 herbivorous Anatidae: effects of sward height, body mass and bill size. *Journal of Animal Ecology*
437 72, 220-231.
- 438 Dussault, C., Ouellet, J.P., Courtois, R., Huot, J., Breton, L., Jolicoeur, H., Kelt, D., 2005. Linking
439 Moose Habitat Selection to Limiting Factors. *Ecography* 28, 619-628.
- 440 Eklundh, L., Jönsson, P., 2015. TIMESAT 3.2 Software Manual. Lund and Malmö University,
441 Sweden.
- 442 Ely, C.R., 1992. Time Allocation by Greater White-Fronted Geese: Influence of Diet, Energy
443 Reserves and Predation. *Condor* 94, 857-870.
- 444 Frich, P., Alexander, L., Dellamarta, P., Gleason, B., Haylock, M., Klein Tank, A., Peterson, T.,
445 2002. Observed coherent changes in climatic extremes during the second half of the twentieth
446 century. *Climate Research* 19, 193-212.
- 447 Fryxell, J.M., 1991. Forage quality and aggregation by large herbivores. *Am. Nat.* 138, 478-498.
- 448 Garrouette, E.L., Hansen, A.J., Lawrence, R.L., 2016. Using NDVI and EVI to Map Spatiotemporal
449 Variation in the Biomass and Quality of Forage for Migratory Elk in the Greater Yellowstone

450 Ecosystem. *Remote Sensing* 8, 404.

451 Gong, P., Wang, J., Yu, L., Zhao, Y., Zhao, Y., Liang, L., Niu, Z., Huang, X., Fu, H., Liu, S., Li, C.,
452 Li, X., Fu, W., Liu, C., Xu, Y., Wang, X., Cheng, Q., Hu, L., Yao, W., Zhang, H., Zhu, P., Zhao, Z.,
453 Zhang, H., Zheng, Y., Ji, L., Zhang, Y., Chen, H., Yan, A., Guo, J., Yu, L., Wang, L., Liu, X., Shi,
454 T., Zhu, M., Chen, Y., Yang, G., Tang, P., Xu, B., Giri, C., Clinton, N., Zhu, Z., Chen, J., Chen, J.,
455 2013. Finer resolution observation and monitoring of global land cover: first mapping results with
456 Landsat TM and ETM+ data. *International Journal of Remote Sensing* 34, 2607-2654.

457 Gottschalk, T.K., Huettmann, F., Ehlers, M., 2005. Thirty years of analysing and modelling avian
458 habitat relationships using satellite imagery data: a review. *International Journal of Remote*
459 *Sensing* 26, 2631-2656.

460 Guan, L., Lei, J.L., Zuo, A.J., Zhang, H., Lei, G.C., Wen, L., 2016. Optimizing the timing of water
461 level recession for conservation of wintering geese in Dongting Lake, China. *Ecol. Eng.* 88, 90-
462 98.

463 Hassall, M., 2001. Foraging Behaviour of Brent Geese, *Branta b. bernicla*, on Grasslands: Effects
464 of Sward Length and Nitrogen Content. *Oecologia* 127, 97-104.

465 Heuermann, N., van Langevelde, F., van Wieren, S.E., Prins, H.H.T., 2011. Increased searching
466 and handling effort in tall swards lead to a Type IV functional response in small grazing herbivores.
467 *Oecologia* 166, 659-669.

468 Hutto, R.L., 1985. Habitat selection by nonbreeding, migratory land birds, *Habitat Selection in*
469 *Birds*. Academic Press, Los Angeles.

470 Ji, L., Gong, P., Geng, X., Zhao, Y., 2015. Improving the Accuracy of the Water Surface Cover
471 Type in the 30 m FROM-GLC Product. *Remote Sensing* 7, 13507-13527.

472 Jiang, Z., Huete, A.R., Didan, K., Miura, T., 2008. Development of a two-band enhanced
473 vegetation index without a blue band. *Remote Sensing of Environment* 112, 3833-3845.

474 Johnson, M.D., Sherry, T.W., 2001. Effects of food availability on the distribution of migratory
475 warblers among habitats in Jamaica. *Journal of Animal Ecology* 70, 546-560.

476 Jönsson, P., Eklundh, L., 2002. Seasonality extraction and noise removal by function fitting to
477 time-series of satellite sensor data. *IEEE Transactions of Geoscience and Remote Sensing* 40,
478 1824-1832.

479 Jönsson, P., Eklundh, L., 2004. Timesat - a program for analyzing time-series of satellite sensor
480 data. *Computers and Geosciences* 30, 833-845.

481 Kays, R., Crofoot, M.C., Jetz, W., Wikelski, M., 2015. Terrestrial animal tracking as an eye on life
482 and planet. *Science* 348, aaa2478.

483 Kerr, J.T., Ostrovsky, M., 2003. From space to species: ecological applications for remote sensing.
484 *Trends in Ecology & Evolution* 18, 299-305.

485 Li, X., Si, Y., Ji, L., Gong, P., 2017. Dynamic response of East Asian Greater White-fronted Geese
486 to changes of environment during migration: Use of multi-temporal species distribution model.
487 *Ecological Modelling* 360, 70-79.

488 Mattocks, J.G., 1971. Goose feeding and cellulose digestion. *Wildfowl* 22, 107-113.

489 Mowat, D.N., Fulkerson, R.S., Tossell, W.E., Winch, J.E., 1965. The in vitro digestibility and
490 protein content of leaf and stem portions of forages. *Canadian Journal of Plant Science* 45, 321-

491 331.
492 Newton, I., 1980. The role of food in limiting bird numbers. *Ardea* 68, 11-30.
493 Pedrana, J., Bustamante, J., Rodriguez, A., Travaini, A., 2011. Primary productivity and
494 anthropogenic disturbance as determinants of Upland Goose *Chloephaga picta* distribution in
495 southern Patagonia. *Ibis* 153, 517-530.
496 Pettorelli, N., Vik, J., Mysterud, A., Gaillard, J., Tucker, C., Stenseth, N., 2005. Using the satellite-
497 derived NDVI to assess ecological responses to environmental change. *Trends in Ecology &*
498 *Evolution* 20, 503-510.
499 Piao, S.L., Fang, J.Y., Zhou, L.M., Ciais, P., Zhu, B., 2006. Variations in satellite-derived
500 phenology in China's temperate vegetation. *Global Change Biology* 12, 672-685.
501 Prop, J., Vulink, T., 1992. Digestion by barnacle geese in the annual cycle - the interplay between
502 retention time and food quality. *Functional Ecology* 6, 180-189.
503 Reed, B.C., Ohlen, D.O., 1994. Measuring phenological variability from satellite imagery. *Journal*
504 *of Vegetation Science* 5, 703-714.
505 Riddington, R., Hassall, M., Lane, S.J., 1997. The selection of grass swards by brent geese *Branta*
506 *b bernicla*: Interactions between food quality and quantity. *Biological Conservation* 81, 153-160.
507 Si, Y., Skidmore, A.K., Wang, T., de Boer, W.F., Toxopeus, A.G., Schlerf, M., Oudshoorn, M.,
508 Zwerver, S., van der Jeugd, H., Exo, K.-M., Prins, H.H.T., 2011. Distribution of Barnacle Geese
509 *Branta leucopsis* in relation to food resources, distance to roosts, and the location of refuges. *Ardea*
510 99, 217-226.
511 Si, Y., Xin, Q., de Boer, W.F., Gong, P., Ydenberg, R.C., Prins, H.H.T., 2015a. Do Arctic breeding
512 geese track or overtake a green wave during spring migration? *Scientific Reports* 5, 8749.
513 Si, Y., Xin, Q., Prins, H.H.T., de Boer, W.F., Gong, P., 2015b. Improving the quantification of
514 waterfowl migration with remote sensing and bird tracking. *Science Bulletin* 60, 1984-1993.
515 Si, Y., Xu, Y., Xu, F., Li, X., Zhang, W., Wielstra, B., Wei, J., Liu, G., Luo, H., Takekawa, J., 2018.
516 Spring migration patterns, habitat use, and stopover site protection status for two declining
517 waterfowl species wintering in China as revealed by satellite tracking. *Ecology & Evolution* 8,
518 6280-6289.
519 Somveille, M., Rodrigues, A.S.L., Manica, A., 2018. Energy efficiency drives the global seasonal
520 distribution of birds. *Nature ecology & evolution* 2, 962-969.
521 Swets, J.A., 1988. Measuring the accuracy of diagnostic systems. *Science* 240, 1285-1293.
522 van der Graaf, A.J., Loonen, M.J.J.E., Engelmoer, M., Drent, R.H., 2002. Short-term and long-
523 term facilitation of goose grazing by livestock in the Dutch Wadden Sea area. *Journal of Coastal*
524 *Conservation* 8, 179-188.
525 van der Graaf, A.J., Stahl, J., Bakker, J.P., 2005. Compensatory growth of *Festuca rubra* after
526 grazing: can migratory herbivores increase their own harvest during staging? *Functional Ecology*
527 19, 961-969.
528 van der Graaf, S.A.J., Stahl, J., Klimkowska, A., Bakker, J.P., Drent, R.H., 2006. Surfing on a
529 green wave - how plant growth drives spring migration in the Barnacle Goose *Branta leucopsis*.
530 *Ardea* 94, 567-577.
531 van der Wal, R., van de Koppel, J., Sagel, M., 1998. On the relation between herbivore foraging

532 efficiency and plant standing crop: an experiment with barnacle geese. *Oikos* 82, 123-130.
533 Wan, Z.M., Dozier, J., 1996. A generalized split-window algorithm for retrieving land-surface
534 temperature from space. *IEEE Trans. Geosci. Remote Sensing* 34, 892-905.
535 Wang, J., Sheng, Y., Tong, T.S.D., 2014. Monitoring decadal lake dynamics across the Yangtze
536 Basin downstream of Three Gorges Dam. *Remote Sensing of Environment* 152, 251-269.
537 Wu, X., Lv, M., Jin, Z., Michishita, R., Chen, J., Tian, H., Tu, X., Zhao, H., Niu, Z., Chen, X., Yue,
538 T., Xu, B., 2014. Normalized difference vegetation index dynamic and spatiotemporal distribution
539 of migratory birds in the Poyang Lake wetland, China. *Ecological Indicators* 47, 219-230.
540 Xie, C., Huang, X., Mu, H.Q., Yin, W., 2017. Impacts of Land-Use Changes on the Lakes across
541 the Yangtze Floodplain in China. *Environmental Science & Technology* 51, 3669-3677.
542 Yu, L., Li, X., Li, C., Zhao, Y., Niu, Z., Huang, H., Wang, J., Cheng, Y., Lu, H., Si, Y., Yu, C., Fu,
543 H., Gong, P., 2017. Using a global reference sample set and a cropland map for area estimation in
544 China. *Science China-Earth Sciences* 60, 277-285.
545 Zhang, W., Li, X., Yu, L., Si, Y., 2018. Multi-scale habitat selection by two declining East Asian
546 waterfowl species at their core spring stopover area. *Ecological Indicators* 87, 127-135.
547 Zhao, M., Cong, P., Barter, M., 2012. The changing abundance and distribution of Greater White-
548 fronted Geese *Anser albifrons* in the Yangtze River floodplain: impacts of recent hydrological
549 changes. *Bird Conservation International* 22, 135-143.